

From Selective Deep Convolutional Features to Compact Binary Representations for Image Retrieval

Thanh-Toan Do*, Tuan Hoang*, Dang-Khoa Le Tan, Ngai-Man Cheung

Abstract—Convolutional Neural Network (CNN) is a very powerful approach to extract discriminative local descriptors for effective image search. Recent work adopts fine-tuned strategies to further improve the discriminative power of the descriptors. Taking a different approach, in this paper, we propose a novel framework to achieve competitive retrieval performance. Firstly, we propose various masking schemes, namely *SIFT-mask*, *SUM-mask*, and *MAX-mask*, to select a representative subset of local convolutional features and remove a large number of redundant features from a feature map. We demonstrate that proposed masking schemes are effectively to address the burstiness issue and improve retrieval accuracy. Secondly, we propose to employ recent embedding and aggregating methods to further enhance feature discriminability. Additionally, we include a hashing module to produce compact binary image representations which are effective for the retrieval. Extensive experiments on six image retrieval benchmarks demonstrate that our proposed framework achieves state-of-the-art retrieval accuracy.

I. INTRODUCTION

Content-based image retrieval (CBIR) has attracted a sustained attention from the multimedia/computer vision community [1], [2], [3], [4], [5] due to its wide range of applications, e.g., visual search, place recognition. Earlier works heavily rely on hand-crafted local descriptors, e.g., SIFT [6] and its variant [7]. Even though there are great improvements of the SIFT-based image search systems over time, the performance of these systems still has room for improvement. There are two main issues: the first and the most important one is that SIFT features lack discriminability [8] to emphasize the differences in images. Even though this drawback is relieved to some extent when embedding local features to much higher dimensional space [9], [10], [11], [12], [13], [14], there is still a large semantic gap between SIFT-based image representation and human perception on instances (objects/scenes) [8]. Secondly, the strong effect of *burstiness* [15], i.e., numerous descriptors are almost similar within the same image, considerably degrade the quality of SIFT-based image representation for the image retrieval task [11], [15], [16].

Recently, deep Convolutional Neural Networks (CNN) have achieved a lot of success in various problems including image classification [17], [18], [19], [20], object detection [21], [22], [23], [24], semantic segmentation [25], [26], [27] etc. After training a CNN on a huge annotated dataset, e.g., ImageNet

[28], outputs of middle/last layers can capture rich information at higher semantic levels. On one hand, the output of the deeper layer possesses abstract understanding of images for computer vision tasks that require high-invariance to the intra-class variability, e.g., classification, detection [17], [18], [19], [20], [21], [22]. On the other hand, the middle layers contain more visual information on edges, corners, patterns, and structures. Therefore, they are more suitable for image retrieval. Utilizing the outputs of the convolutional layers to produce the image representation, recent image retrieval methods [8], [29], [30], [31], [32], [33] achieve a considerable performance boost.

Although the local convolutional (conv.) features are more discriminative than SIFT features [8], to the best of our knowledge, none of previous works has considered the burstiness problem which may appear in the local conv. features. In this paper, focusing on CNN-based image retrieval, we delve deeper into the issue: “*How to eliminate redundant local features in a robust way?*” Since elimination of redundant local features leads to better representation and faster computation, we emphasize both aspects in our experiments. Specifically, inspired by the concept of finding a set of interest regions before deriving their corresponding local features — the concept which has been used in design of hand-crafted features, we propose three different masking schemes for selecting *representative* local conv. features, including *SIFT-mask*, *SUM-mask*, and *MAX-mask*. The principal ideas of our main contribution are that we take advantages of SIFT detector [6] to produce SIFT-mask; moreover, we utilize sum-pooling and max-pooling over all conv. feature channels to derive SUM-mask and MAX-mask, respectively.

Additionally, most of the recent works, which take local conv. features as input [30], [29], [34], do not leverage local feature embedding and aggregating [10], [11], [12], [13], which are effective processes to enhance the discriminability for hand-crafted features. In [8], the authors mentioned that the deep convolutional features are already discriminative enough for image retrieval task; hence, the embedding is not necessary to enhance their discriminability. However, in this work, we find that by utilizing the state-of-art embedding and aggregating methods on our selected deep convolutional features [12], [13], [11], [10], we can significantly enhance the discriminability of the representations. Our experiments show that by applying embedding and aggregating on our selected local conv. features, the aggregated representations significantly improve image retrieval accuracy.

Thanh-Toan Do is with The University of Adelaide, Australia. Tuan Hoang, Dang-Khoa Le Tan, Ngai-Man Cheung are with Singapore University of Technology and Design, Singapore.

* indicates equal contribution.

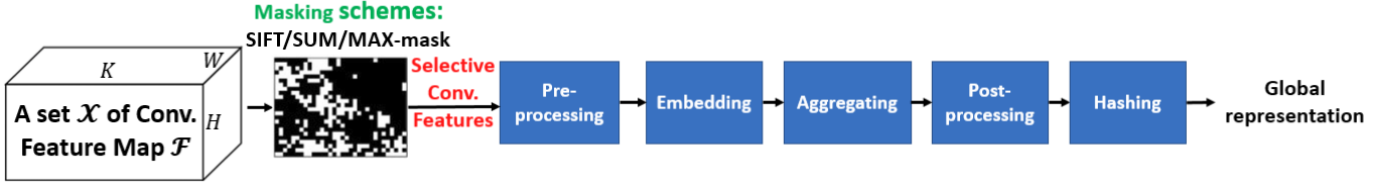


Fig. 1: The overview of our proposed framework to produce discriminative global binary representations.

Furthermore, we also further push the proposed system to achieve compact binary codes by cascading a state-of-the-art unsupervised hashing method, e.g., Iterative Quantization (ITQ) [35] or Relaxed Binary Autoencoder (RBA) [36] into the system. The binary representations would help to achieve significant benefits in retrieval speed and memory consumption. The overview of the proposed framework is shown in Fig. 1.

A preliminary version of this work which introduces the proposed masking schemes has been presented in [37]. In the current version, we provide deeper analysis to explain how various masking schemes work and then we further optimize the framework to solve two crucial problems for large scale image search, i.e., searching speed and storage. Specifically, we propose to cascade a state-of-the-art unsupervised hash function into the framework to further binarize real-valued aggregated representations to binary representations which would allow the fast searching and sufficient storage. In addition, we also conduct very large scale experiments, i.e., on Flickr1M dataset [38], which consists of one million images. The experiments on such kind of large scale dataset confirms the effectiveness of the proposed method for real applications which usually have to deal with very large scale datasets. We also conduct more experiments to deeply analyze the effectiveness of the proposed framework and to extensively compare to the state of the art. The extensive experiments on six benchmark datasets show that the proposed framework significantly outperforms the state of the art when images are represented by either real-valued representations or compact binary representations.

The remainder of this paper is organized as follows. Section II discusses related works. Section III presents the details of the proposed masking schemes for selecting a set of representative local conv. features, together with empirical analysis to justify their effectiveness. Section IV presents the proposed framework for computing the final image representation which takes selected local deep conv. features as input and output a global fixed-length image representation. Section V presents a wide range of experiments to comprehensively evaluate our proposed framework. Section VI concludes the paper.

II. RELATED WORK

In the last few years, image retrieval has witnessed an increasing of performance due to the use of better image representations, i.e., deep features obtained from pre-trained CNN models, which are trained on image classification task. The early CNN-based work [39] directly used deep fully connected activations for the image retrieval. In stead of

directly using features from the pre-trained networks for the retrieval as [39], other works apply different processings on the pre-trained features to enhance the discriminability. Gong et al. [40] proposed Multi-Scale Orderless Pooling (MOP) to embed and pool the CNN fully-connected activations of image patches of an image at different scale levels. This enhances the scale invariant of the extracted features. However, the method is computationally expensive because multiple patches (resized to the same size) of an image are fed forward into the CNN. The recent work [41] suggested that CNN fully-connected activations and SIFT features are highly complementary. They proposed to integrate SIFT features with fully-connected CNN features at different levels. Concurrently, Liu et al. [42] proposed ImageGraph to fuse various types of features, e.g., CNN fully-connected features, BoW on SIFT [6] descriptors, HSV color histogram, and GIST features [43]. This method even though achieves very good performances, it requires very high-dimensional features. Furthermore, ImageGraph must be built on database images, which may be prohibitive on large scale datasets.

Later works shift the focus from fully-connected layers to conv. layers for extracting image features for the retrieval problem because lower layers are more general and certain level of spatial information is still preserved [44]. When conv. layers are used, the conv. features are usually considered as local features, hence, a pooling method (sum or max) is applied on the conv. features to produce the single image representation. Babenko and Lempitsky [8] showed that sum-pooling outperforms max-pooling when the final image representation is whitened. Kalantidis et al. [29] further improved sum-pooling on conv. features by proposing a non-parametric method to learn weights for both spatial locations and feature channels. Tolias et al. [30] revisited max-pooling by proposing the strategy to aggregate the maximum activation over multiple spatial regions sampled on a conv. layer using a fixed layout.

In stead of using pre-trained features (with / without additional processing) for the retrieval task, In [45], Babenko et al. showed that fine-tuning an off-the-shelf network (e.g., AlexNet [17] or VGG [18]) can enhance the discriminability of the deep features [45] for image retrieval. However, the collecting of labeled training data is non-trivial [45]. Recent works tried to overcome this challenge by proposing unsupervised/weakly-supervised fine-tuning approaches which are specific for image retrieval. Arandjelovic et al. [31] proposed a new generalized VLAD layer and this layer can be stacked to any CNN architecture. The whole architecture, named NetVLAD, is trained in an end-to-end fashion in which the data is collected in a weakly-supervised manner from Google Street View Time

Machine. Also taking the approach of fine-tuning the network in a weakly-supervised manner, Cao et al. [46] proposed an automatic method to harvest data from Flickr with GPS information to form GeoPair dataset [47]. The dataset is used to train a special architecture called Quartet-net with the novel double margin contrastive loss function. Concurrently, Radenovic et al. [34] proposed a different approach to fine-tune state-of-the-art CNNs of classification task for image retrieval. They take advantages of 3D reconstruction to obtain matching / non-matching pairs of images in an unsupervised manner for fine-tuning process.

In regards to compact image representations, the earlier work [48] presented feature dimension selection on embedded high-dimensional features as a compression method to achieve compact representations. Radenovic et al. [34], [49] later introduced to learn the whitening and dimensionality reduction in the supervised manner resulting in better performances than baseline PCA method. Albert et al. [50] made use of the product quantization [51] to compress image representations. This approach even though achieves good accuracy, it is not as efficient as the hashing approach, which we utilize in this paper, in term of retrieval time [52]. Do et al. [36] proposed to produce binary representations by simultaneously aggregating raw local features and hashing. Differentially, in this paper, we proposed various masking schemes in combination with a complete framework to produce more discriminative binary representations.

III. SELECTIVE LOCAL DEEP CONV. FEATURES

In this section, we first define the set of local deep conv. features which we work on throughout the paper (Section III-A). We then present proposed strategies for selecting a subset of discriminative local conv. features, including **SIFT-mask**, **SUM-mask**, and **MAX-mask** (Section III-B). Finally, we discuss experiments to confirm the effectiveness of the proposed methods (Section III-C).

A. Local deep convolutional features

We consider a pre-trained CNN in which all fully connected layers are discarded. Given an input image I of size $W_I \times H_I$ that is fed through a CNN, the 3D activations (responses) tensor of a conv. layer has the size of $W \times H \times K$ dimensions, where K is the number feature maps and $W \times H$ is the spatial resolution of the feature map. We consider this 3D tensor of responses as a set \mathcal{X} of $(W \times H)$ local features; each of them has K dimensions. In other words, each position on the $W \times H$ spatial grid is the location of a local feature. Each local conv. feature is a vector of K values of the K feature maps at a particular location. We denote $\mathcal{F}^{(k)}$ as k^{th} feature map (and its size is $W \times H$). Note that the choice of the conv. layer to be used is not fixed in our method. We investigate the impact of choosing different conv. layers in Section V.

B. Selective features

We now formally propose different methods to compute a selection mask, i.e. a set of unique coordinates $\{(x, y)\}$

in the feature maps where local conv. features are retained ($1 \leq x \leq W; 1 \leq y \leq H$). Our proposed methods for selecting discriminative local deep conv. features are inspired by the concept of finding the interest regions in the input images which is traditionally used in the design of hand-crafted features.

1) **SIFT-Mask**: Prior the emergence of CNN features in the image retrieval task, most previous works [12], [13], [15], [11], [10], [53], [54], [16] are based on SIFT [6] features and its variant RootSIFT [7]. Even though it has been showed that there is still a gap between SIFT-based representation and the semantic meaning in the image, these works have clearly demonstrated the capability of SIFT feature, especially in the aspect of key-point detection. Fig. 2 - Row (2) show local image regions which are covered by SIFT. We can observe that regions covered by SIFT mainly focus on the salient regions, i.e., buildings. This means that SIFT keypoint detector is capable to locate important regions of images. Hence, we propose a method which takes advantage of SIFT detector in combination with highly-semantic local deep conv. features. We will discuss more about the SIFT-mask in Section III-C.

Specifically, let set $\mathcal{S} = \{(x^{(i)}, y^{(i)})\}_{i=1}^n$ be SIFT feature locations extracted from an image with the size of $W_I \times H_I$; $1 \leq x^{(i)} \leq W_I$, $1 \leq y^{(i)} \leq H_I$. Based on the fact that convolutional layers still preserve the spatial information of the input image [30], we select locations on the spatial grid $W \times H$ (of the feature map) which correspond to locations of SIFT key-points, i.e.,

$$\mathcal{M}_{\text{SIFT}} = \left\{ \left(x_{\text{SIFT}}^{(i)}, y_{\text{SIFT}}^{(i)} \right) \right\} \quad i = 1, \dots, n; \quad (1)$$

where $x_{\text{SIFT}}^{(i)} = \text{round} \left(\frac{x^{(i)} W}{W_I} \right)$ and $y_{\text{SIFT}}^{(i)} = \text{round} \left(\frac{y^{(i)} H}{H_I} \right)$, in which $\text{round}(\cdot)$ represents rounding to nearest integer. By keeping only locations $\mathcal{M}_{\text{SIFT}}$, we expect to remove “background” deep conv. features, while keeping “foreground” ones.

2) **MAX-Mask**: It is known that each feature map contains the activations of a specific visual structure [55], [21]. Hence, we propose to select a subset of local conv. features which contains high activations for all visual contents, i.e., we select the local features that capture the most prominent structures in the input images. This property, actually, is desirable to distinguish scenes.

Specifically, we assess each feature map and select the location corresponding to the max activation value on that feature map. Formally, we define the selected locations \mathcal{M}_{MAX} as follows:

$$\mathcal{M}_{\text{MAX}} = \left\{ \left(x_{\text{MAX}}^{(k)}, y_{\text{MAX}}^{(k)} \right) \right\} \quad k = 1, \dots, K; \quad (2)$$

$$\left(x_{\text{MAX}}^{(k)}, y_{\text{MAX}}^{(k)} \right) = \arg \max_{(x, y)} \mathcal{F}_{(x, y)}^{(k)}.$$

3) **SUM-Mask**: Departing from the MAX-mask idea, we propose a different masking method based on the motivation that a local conv. feature is more *informative* if it gets excited in more feature maps, i.e., the sum on description values of a local feature is larger. By selecting local features that have large values of sum, we can expect that those local conv. features contain a lot of information from different local image

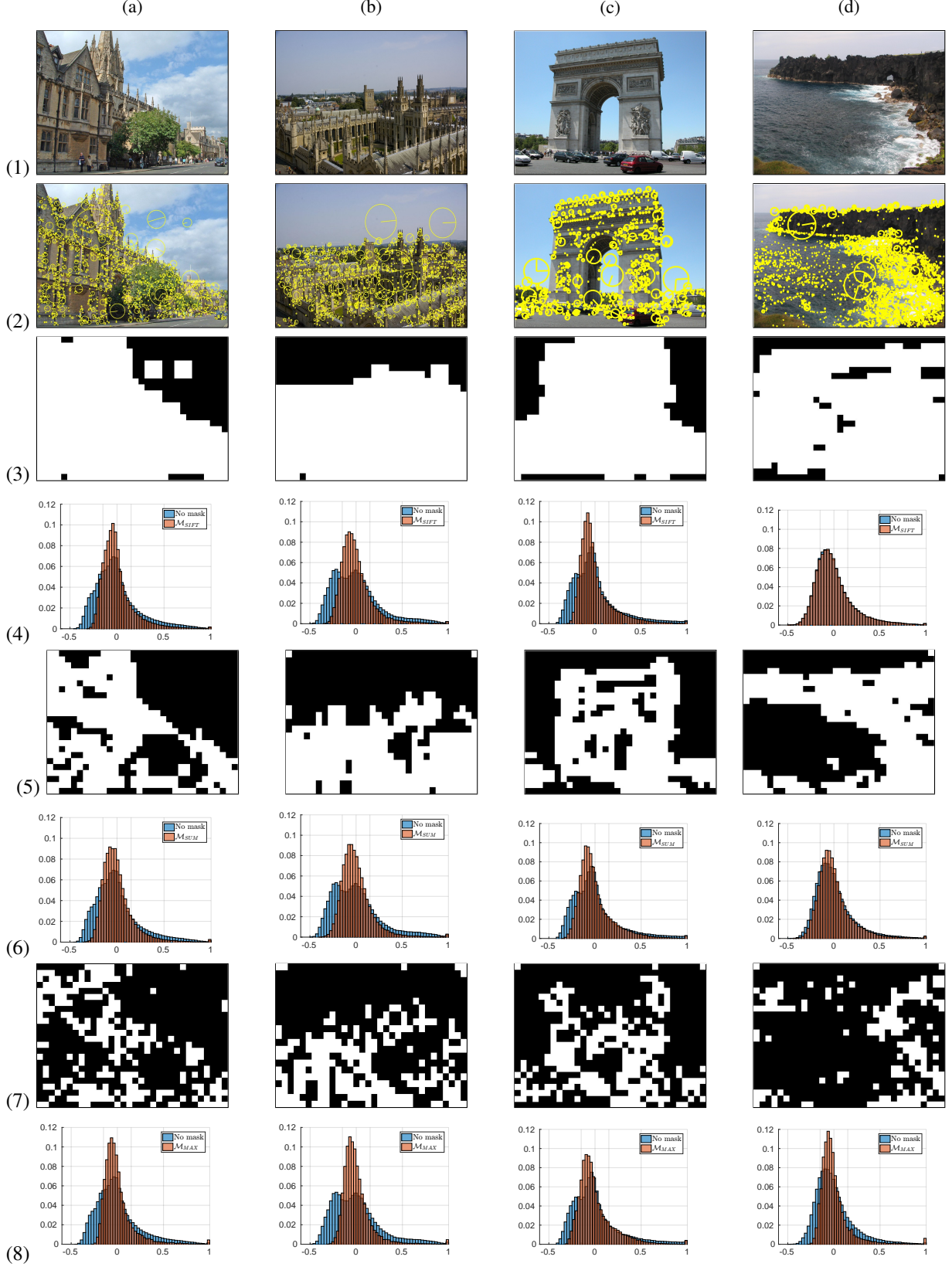


Fig. 2: Examples of masks to select local features. The original images are showed on the first row. The second row shows regions which are covered by SIFT features. The SIFT/SUM/MAX-masks of corresponding images (in the 1st row) are showed in the 3rd, 5th, and 7th rows. The normalized histograms of covariances of sets of local conv. features with/without applying masks are shown in the 4th, 6th, and 8th rows.

structures [55]. Formally, we define the selected locations \mathcal{M}_{SUM} as follows:

$$\begin{aligned} \mathcal{M}_{\text{SUM}} &= \left\{ (x, y) \mid \Sigma_{(x,y)}^{\mathcal{F}} \geq \alpha \right\}, \\ \Sigma_{(x,y)}^{\mathcal{F}} &= \sum_{k=1}^K \mathcal{F}_{(x,y)}^{(k)}, \quad \alpha = \text{median}(\Sigma^{\mathcal{F}}). \end{aligned} \quad (3)$$

C. Effectiveness of masking schemes

In this section, we deeply analyze the effectiveness of the proposed masking schemes, in both qualitative and quantitative results.

SIFT detector [6] is designed to detect interesting points which are robust with changes in image scale, noise and illumination; therefore, these interesting points usually lie on high-contrast regions of images, e.g., corners. These regions also usually contain detail structures of the scenes which are necessary in differentiating scenes. While smooth regions, e.g., sky, road surfaces, are ignored as these regions are mainly background and contribute very little information. Hence, by using the SIFT-mask, we expect to select local conv. features at higher-contrast, i.e. potentially informative regions. However, there are two main issues when using the SIFT-mask: (i) in cases of blurry images, the SIFT detector unsurprisingly fails to locate informative regions. (ii) However, having too many interesting points also causes unexpected outcomes, which is known as the burstiness effect [15], i.e., too many redundant local features are selected. For example, in Fig. 2-(2d)¹ and 2-(3d), SIFT-mask includes almost all local features of the sea regions, which are obviously redundant.

On the other hand, SUM/MAX-masks perform much better when selecting just a few features at the sea region, i.e. Fig. 2-(5d) and 2-(7d) respectively, which are necessary to distinguish scenes with and without sea, and not to cause a serious burstiness effect which potentially makes the distinguishing different scenes with sea regions difficult. In fact, the burstiness effect is the main reason explaining why SIFT-mask underperforms SUM/MAX-mask rather than due to SIFT-mask fails to select important regions, which is also confirmed by the two facts: (i) SUM/MAX-masks are mainly subsets of SIFT-mask, and (ii) applying SIFT-mask helps to improve performances (compared to no mask) which means that important regions have been selected, otherwise performances will drop. Note that the empirical results will be presented in Section V-B1. It is worth nothing that, regarding local conv. features, the burstiness effect is expected to be less severe since local conv. features have much larger receptive fields than those of SIFT features. For examples, a local conv. feature from pool5 layers of AlexNet [17] and VGG16 [18] covers a region of 195×195 and 212×212 in the input image, respectively. We will further investigate this effect in Section IV-D.

Comparing SUM-mask and MAX-mask, which are computed from learned features, they both have the capability of detecting important regions based on the responded activation of regions. However, their principles of selecting local

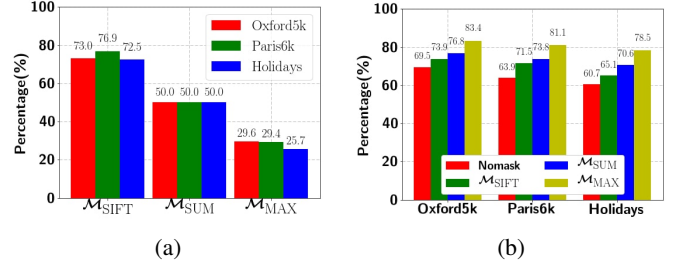


Fig. 3: Fig. 3a: The averaged percentage of remaining local conv. features after applying masks. Fig. 3b: The averaged percentage of the covariance values in the range of $[-0.15, 0.15]$.

features are different. In particular, given prominent regions, the corresponding local conv. features of those regions are usually highly activated. As a result, the sums on those features are larger. This fact explains why SUM-mask more densely selects local conv. features at prominent regions. However, as the receptive fields of neighbouring features are largely overlapping, they are likely to contain similar information, i.e., redundant. On the other hand, MAX-mask only selects the features which have highest activation values. Hence, we expect MAX-mask can select the best features for representing the visual structures of prominent regions. As a result, we minimize the chance of selecting multiple similar local features.

In addition, we quantitatively evaluate the effectiveness of our proposed masking schemes in eliminating redundant local conv. features. Firstly, Figure 3a shows the averaged percentage of the remaining local conv. features after applying our proposed masks on three datasets: *Oxford5k* [56], *Paris6k* [57], and *Holidays* [58]. Clearly, there are a large number of local conv. features removed, about 25%, 50%, and 70% for SIFT/SUM/MAX-mask respectively. Additionally, we present the normalized histograms of covariances of selected local conv. features after applying different masks in Fig. 2-Row 4th, 6th, and 8th. To compute the covariances, we first l_2 -normalize local conv. features, which are extracted from pool5 layer of the pre-trained VGG [18] (the input image is of size $\max(W_I, H_I) = 1024$). We then compute the dot products for all pairs of features. For easy comparison, we include the normalized histograms of covariances of all available local conv. features (i.e., before masking). These figures clearly show that the distributions of covariances after applying masks have much higher peaks around 0 and have smaller tails than those without applying masks. This indicates some reduction of correlation between the features with the use of masks. Furthermore, Fig. 3b shows the averaged percentage of l_2 -normalized feature pairs that have dot products in the range of $[-0.15, 0.15]$. The chart shows that the selected features are more uncorrelated. In summary, Fig. 3 suggests that our proposed masking schemes can help to remove a large proportion of redundant local conv. features, hence achieving a better representative set of local conv. features. Note that with the reduced number of features, we can reduce computational cost, e.g., the embedding and aggregating of features in the subsequent steps.

¹Row (2) and column (d) of Fig. 2.

IV. FRAMEWORK: EMBEDDING AND AGGREGATING ON SELECTIVE CONV. FEATURES

A. Pre-processing

Given a set $\mathcal{X}_{\mathcal{M}} = \{\mathbf{x}_{(x,y)} \mid (x,y) \in \mathcal{M}_*\}$, where $\mathcal{M}_* \in \{\mathcal{M}_{\text{SUM}}, \mathcal{M}_{\text{MAX}}, \mathcal{M}_{\text{SIFT}}\}$ of selective K -dimensional local conv. features belonged to the set, we apply the principal component analysis (PCA) to compress local conv. features to smaller dimension d : $\mathbf{x}^{(d)} = M_{\text{PCA}}\mathbf{x}$, where M_{PCA} is the PCA-matrix. There are two reasons for this dimensional reduction operation. Firstly, the lower dimensional local features help to produce compact final image representation as done in state-of-the-art image retrieval systems [8], [30], [34]. Secondly, applying PCA could help to remove noise and redundancy; hence, enhancing the discrimination. We subsequently $l2$ -normalize the compressed local conv. features.

B. Embedding

In this section, we aim to enhance the discriminability of selected local conv. features. We propose to accomplish this by embedding the conv. features to higher-dimensional space: $\mathbf{x} \mapsto \phi(\mathbf{x})$, using state-of-the-art embedding methods: *Fisher vector* – FV [10], *vector of locally aggregated descriptors* – VLAD [11], *triangulation embedding* – Temb [12], *function approximation-based embedding* – F-FAemb [14]. It is worth noting that while in [8], the authors mentioned that applying embedding on the *original* set of local deep conv. features does not necessary enhance the discriminative power of the features. In this work, we find that applying the embedding on the set of *selected* features significantly improves their discriminability.

This section briefly describe embedding methods used in our work, i.e., FV [10], VLAD [11], Temb [12], F-FAemb [14]. Note that in the original design of FV and VLAD, the embedding and the aggregation (i.e., sum aggregation) are integrated in a unified formulation. This prevents the using of recent state-of-the-art aggregations (e.g., democratic pooling [12]) on the embedded vectors produced by FV, VLAD. Hence, in order to make the embedding and the aggregating flexible, we follow [14], i.e., decomposing the formulation of VLAD and FV. Specifically, we apply the embedding on each local feature separately. This allows different aggregating methods to be applied on the embedded features.

For clarity, we pre-define the codebook of visual words learning by Gaussian Mixture Model used in Fisher Vector method as $\mathcal{C}_{\mathbf{G}} = \{\mu_i; \Sigma_i; w_i\}_{i=1}^k$, where w_i , μ_i , and Σ_i denote respectively the weight, mean vector, and covariance matrix of the i -th Gaussian. Similarly, the codebook learning by K-means used in VLAD, Temb, and F-FAemb methods are defined as $\mathcal{C}_{\mathbf{K}} = \{c_j\}_{j=1}^k$, where c_j is a centroid.

Fisher Vector (FV) [10] produces a high-dimensional vector representation of $(2 \times k \times d)$ -dimension when considering both 1-st and 2-nd order statistic of the local features.

$$\begin{aligned} \phi_{\text{FV}}(\mathbf{x}) &= [\cdots, u_i^T, \cdots, v_i^T, \cdots]^T \quad i = 1, \cdots, k; \\ u_i &= \frac{p_i(\mathbf{x})}{\sqrt{w_i}} \left(\frac{\mathbf{x} - \mu_i}{\sigma_i} \right), \quad v_i = \frac{p_i(\mathbf{x})}{\sqrt{2w_i}} \left[\left(\frac{\mathbf{x} - \mu_i}{\sigma_i} \right)^2 - 1 \right]. \end{aligned} \quad (4)$$

Where $p_i(\mathbf{x})$ is the posterior probability capturing the strength of relationship between a sample \mathbf{x} and the i -th Gaussian model and $\sigma_i = \sqrt{\text{diag}(\Sigma_i)}$.

VLAD [11] is considered as a simplification of the FV. It embeds \mathbf{x} to the feature space of $(d \times k)$ -dimension.

$$\phi_{\text{VLAD}}(\mathbf{x}) = [\cdots, q_i(\mathbf{x} - c_i)^T, \cdots]^T \quad i = 1, \cdots, k. \quad (5)$$

Where c_i is the i -th visual word of the codebook $\mathcal{C}_{\mathbf{K}}$, $q_i = 1$ if c_i is the nearest visual word of \mathbf{x} and $q_i = 0$ otherwise.

Temb [12]. Different from FV and VLAD, Temb avoids the dependency on absolute distances by only preserve direction information between a feature \mathbf{x} and visual words $c_i \in \mathcal{C}_{\mathbf{K}}$.

$$\phi_{\Delta}(\mathbf{x}) = \left[\cdots, \left(\frac{\mathbf{x} - c_i}{\|\mathbf{x} - c_i\|} \right)^T, \cdots \right]^T \quad i = 1, \cdots, k. \quad (6)$$

F-FAemb [14]. Departing from the idea of linearly approximation of non-linear function in high dimensional space, the authors showed that the resulted embedded vector of the approximation process is the generalization of several well-known embedding methods such as VLAD [11], TLCC [59], VLAT [60]. Let

$$s_i = \gamma_i(\mathbf{x}) V \left((\mathbf{x} - c_i)(\mathbf{x} - c_i)^T \right) \quad i = 1, \cdots, k; \quad (7)$$

where $\gamma_i(\mathbf{x})$ is coefficient corresponding to visual word c_i achieved by the function approximation process and $V(\cdot)$ is a function that flattens a matrix to a vector. The $\phi_{\text{F-FAemb}}$ is computed by

$$\phi_{\text{F-FAemb}}(\mathbf{x}) = [\cdots, s_i, \cdots]^T \quad i = 1, \cdots, k. \quad (8)$$

C. Aggregating

Let $\mathbf{V}_i = [\phi(\mathbf{x}_1^i), \cdots, \phi(\mathbf{x}_{n_i}^i)]$ be an $D \times n_i$ matrix that contains n_i D -dimensional embedded local descriptors of i -th image. Sum/average-pooling and max-pooling are two common methods for aggregating this set to a single global feature.

When using the features generating from the activation function, e.g. ReLU [17], of a CNN, **sum/average-pooling** (ψ_s/ψ_a) lack discriminability because they average the high activated outputs by less activated outputs. Consequently, they weaken the effect of highly activated features. **Max-pooling** (ψ_m), on the other hand, is more preferable since it only retains the high activation for each visual content. However, it is worth noting that in practical, the max-pooling is only successfully applied when features are sparse [61]. For examples, in [30], [34], the max-pooling is applied on each feature map because there are few of high activation values in a feature map. When the embedding is applied to embed local features to high dimensional space, the max-pooling may be failed since the local features are no longer sparse [61].

H. Jégou et al. [12] introduced **democratic aggregation** (ψ_d) method applied to image retrieval problem. The main idea of democratic aggregation is to equalize the similarity between each local embedded vector and the aggregated representation. Note that, concurrently, Murray and Perronnin [62] proposed **Generalized Max Pooling (GMP)** (ψ_{GMP}), which shares the similar idea with *democratic aggregation*.

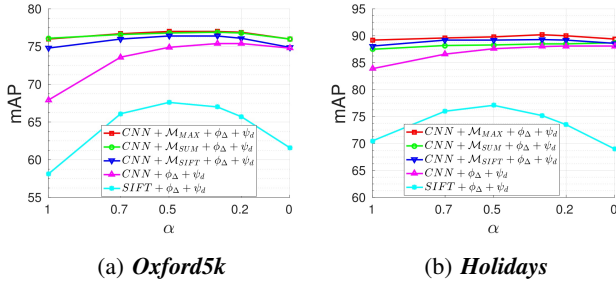


Fig. 4: Impact of power-law normalization factor α on **Oxford5k** and **Holidays** datasets. Following the setting in [12], we set $d = 128$ and $|\mathcal{C}| = 64$ for both SIFT and conv. features. The local conv. features are extracted from pool15 layer of the pre-trained VGG [18].

Democratic aggregation can work out-of-the-box with various embedded features such as VLAD [11], Fisher vector [10], Temb [12], FAemb [13], F-FAemb [14], and it has been shown to outperform sum-pooling in term of retrieval performance with embedded hand-crafted SIFT features [12]. Noted that democratic aggregation requires local features to be l_2 -normalized.

D. Post-processing

Power-law normalization (PN). The *burstiness* of visual elements [15], which is numerous descriptors are almost similar within the same image, is known as a major drawback of hand-crafted local descriptors, e.g., SIFT [6]. As a result, this phenomenon strongly affects the measure of similarity between two images. By applying power-law normalization [63] to the final image representation ψ and subsequently l_2 -normalization, it has been shown to be an efficient way to reduce the effect of burstiness [12]. The power-law normalization formula is given as $PN(x) = \text{sign}(x)|x|^\alpha$, where $0 \leq \alpha \leq 1$ is a constant [63].

However, to the best of our knowledge, no previous work has re-evaluated the *burstiness* phenomena on the local conv. features. Figure 4 shows the analysis of PN effect on local conv. features using various proposed masking schemes. This figure shows that the local conv. features ($CNN + \phi_\Delta + \psi_\Delta$) are still affected by the burstiness: the retrieval performance changes when applying PN. The figure also shows that the burstiness has much stronger effect on SIFT features ($SIFT + \phi_\Delta + \psi_\Delta$) than conv. features. The proposed SIFT, SUM and MAX masks help reduce the burstiness effect significantly: the PN has less effect on $CNN + \mathcal{M}_{MAX/SUM/SIFT} + \phi_\Delta + \psi_\Delta$ than on $CNN + \phi_\Delta + \psi_\Delta$. This confirms the capability of removing redundant local features of our proposed masking schemes. Similar to previous works, we set $\alpha = 0.5$ in our later experiments, unless stated otherwise.

Rotation normalization and dimension reduction (RN). The power-law normalization suppresses visual burstiness but not frequent co-occurrences which also corrupt the similarity measure [53]. In order to reduce the effect of co-occurrences, we follow [53], [12] to rotate data with a whitening matrix learned from the aggregated vectors of the training set.

E. Hashing function

In the large scale image retrieval problem, binary hashing, where images are represented by a L -bit binary codes, is an attractive approach because the binary representations allow the fast searching and sufficient storage.

There is a wide range of hashing methods have been proposed in the literature, in both unsupervised and supervised [64], [65]. Although supervised hashing methods usually outperform unsupervised hashing methods on some specific retrievals in which the data is labeled, they are not suitable for the general image retrieval (which is focused in this work). That is because in the general image retrieval, the label of an image is not well defined. Most of general image retrieval benchmarks, e.g., Holidays, Oxford5k, Paris6k, does not have labeled training data. On the other hand, the unsupervised hashing is well suitable for the general image retrieval task. Unsupervised hashing methods do not require the data label for training. Most of unsupervised hashing methods tries to preserve the geometric structure of data by using reconstruction criterion [35], [66], [36], [67] or directly preserving the distance similarity between samples [68], [69]. By above reasons, we propose to cascade a state-of-the-art unsupervised hash function, i.e., Iterative Quantization (ITQ) [35], K-mean Hashing (KMH) [70], or Relaxed Binary Autoencoder (RBA) [36], into the framework to further binarize the real-valued aggregated representations to binary representations.

The overview of our proposed framework is shown in Fig. 1. In the next section, we will conduct extensive experiments to evaluate the framework in both cases: real-valued global representations (i.e., without the hash function in the framework), and binary global representations (i.e., with the hash function in the framework).

V. EVALUATION

In this section, we conduct comprehensive experiments to evaluate the proposed framework on six standard image retrieval benchmark datasets, including INRIA Holidays [58] dataset, Oxford5k dataset [56], Paris6k dataset [57], Oxford105k dataset [56], Paris106k dataset [57], and Holidays+Flickr1M dataset [38].

A. Datasets, evaluation protocols, and implementation notes

INRIA Holidays dataset: The *Holidays* dataset [58] contains 1,491 images corresponding to 500 groups of the same scenes. The query image set consists of one image from each group. We also manually rotate images (by ± 90 degrees) to fix the wrong image orientation as in [45], [8], [29].

Oxford Buildings dataset: The *Oxford5k* dataset [56] consists of 5,063 images of buildings and 55 query images corresponding to 11 distinct buildings in Oxford. Each query image contains a bounding box indicating the region of interest. Following the standard protocol [12], [14], [30], [71], we use the cropped query images based on provided bounding boxes.

Paris dataset: The *Paris6k* dataset [57] consists of 6412 images of famous landmarks in Paris. Similar to *Oxford5k*,

TABLE I: Notations and their corresponding meanings. \mathcal{M}, ϕ, ψ denote masking, pooling, and embedding, respectively.

Notation	Meaning	Notation	Meaning
$\mathcal{M}_{\text{SIFT}}$	SIFT-mask	ψ_a	Average-pooling
\mathcal{M}_{SUM}	SUM-mask	ψ_s	Sum-pooling
\mathcal{M}_{MAX}	MAX-mask	ψ_d	Democratic-pooling [12]
ϕ_{FV}	FV [10]	ϕ_{VLAD}	VLAD [11]
ϕ_{Δ}	Temb [12]	$\phi_{\text{F-FAemb}}$	F-FAemb [14]

this dataset has 55 queries corresponding to 11 landmarks. We also use provided bounding boxes to crop the query images accordingly.

Oxford105k and Paris106k datasets: We additionally use 100k Flickr images [56] in combination with *Oxford5k* and *Paris6k* to compose *Oxford105k* and *Paris106k*, respectively. This 100k distractors allow evaluating retrieval methods at a larger scale.

Holidays+Flickr1M: In order to evaluate the retrieval on a very large scale, we merge Holidays dataset with 1M negative images downloaded from Flickr [38], forming the Holidays+Flickr1M dataset. This dataset allows us to evaluate real-like scenarios of the proposed framework.

Evaluation protocols: Follow the state of the art [12], [14], [31], [8], [34], [71], the retrieval performance is measured by mean average precision (**mAP**) over query sets for all datasets. In addition, the *junk* images, which are defined as unclear to be relevant or not to a query, are removed from the ranking.

Implementation notes: In the image retrieval task, it is important to use held-out datasets to learn all necessary parameters to avoid overfitting [8], [34], [71]. Follow standard settings in the literature [12], [14], [30], [8], the set of 5,000 Flickr images² is used as the held-out dataset to learn parameters for *Holidays* and *Holidays+Flickr1M*. The *Oxford5k* is used as the learning set for *Paris6k* and *Paris106k*, while the *Paris6k* is used as the learning for *Oxford5k* and *Oxford105k*.

All images are resized so that the maximum dimension is 1,024 while preserving aspect ratios before fed into the CNN. Additionally, as the common practice in recent works [30], [8], [34], [71], the pretrained VGG16 [18] (with Matconvnet toolbox [72]) is used to extract deep convolutional features. In addition, we utilize the VLFeat toolbox [73] for SIFT detector. We summarize the notations in Table I. The implementation of the proposed framework is available at <https://github.com/hnanhtuan/selectiveConvFeature>.

B. Effects of parameters

1) *Framework:* In this section, we conduct experiments to comprehensively compare various embedding and aggregating methods in combination with different proposed masking schemes. In order to make a fair comparison, we empirically set the retained PCA components- d (of local conv. features) and size of the visual codebooks- $|\mathcal{C}|$ such that the produced final aggregation vectors of different methods have the same dimensionality- D . These parameters are presented in Table II.

TABLE II: Configuration of different embedding methods.

Method	PCA- d	$ \mathcal{C} $	D
FV [10]	48	44	$2 \times d \times \mathcal{C} = 4224$
VLAD [11]	64	66	$d \times \mathcal{C} = 4224$
T-emb [12]	64	68	$d \times \mathcal{C} - 128 = 4224$
F-FAemb [14]	32	10	$\frac{(\mathcal{C} - 2) \times d \times (d + 1)}{2} = 4224$

TABLE III: Comparison of different frameworks. For simplicity, we do not include the notations for post-processing steps (PN and RN). The “**Bold**” values indicates the best performance in each masking method and the “Underline” values indicates the best performance across all settings.

	Method	\mathcal{M}_{MAX}	\mathcal{M}_{SUM}	$\mathcal{M}_{\text{SIFT}}$	None
Oxford5k	$\phi_{\text{FV}} + \psi_a$	67.8	65.1	65.5	59.5
	$\phi_{\text{FV}} + \psi_d$	72.2	71.8	72.0	69.6
	$\phi_{\text{VLAD}} + \psi_s$	66.3	65.6	66.4	65.1
	$\phi_{\text{VLAD}} + \psi_d$	69.2	70.5	71.3	69.4
	$\phi_{\Delta} + \psi_d$	<u>75.8</u>	75.7	75.3	73.4
	$\phi_{\text{F-FAemb}} + \psi_d$	75.2	74.7	74.4	73.8
Paris6k	$\phi_{\text{FV}} + \psi_a$	78.4	76.4	75.8	68.0
	$\phi_{\text{FV}} + \psi_d$	84.5	82.2	82.4	76.9
	$\phi_{\text{VLAD}} + \psi_s$	77.7	74.5	76.0	73.2
	$\phi_{\text{VLAD}} + \psi_d$	80.3	79.5	81.3	79.3
	$\phi_{\Delta} + \psi_d$	<u>86.9</u>	84.8	85.3	83.9
	$\phi_{\text{F-FAemb}} + \psi_d$	86.6	85.9	85.6	82.9
Holidays	$\phi_{\text{FV}} + \psi_a$	83.2	80.0	81.5	78.2
	$\phi_{\text{FV}} + \psi_d$	87.8	86.7	87.1	85.2
	$\phi_{\text{VLAD}} + \psi_s$	83.3	82.0	83.6	82.7
	$\phi_{\text{VLAD}} + \psi_d$	85.5	86.4	87.5	86.1
	$\phi_{\Delta} + \psi_d$	<u>89.1</u>	88.1	88.6	87.3
	$\phi_{\text{F-FAemb}} + \psi_d$	88.6	88.4	88.5	86.4

Note that, in original F-FAemb [14] the authors remove the first $d(d+1)/2$ components of the features after aggregating step (Section IV-C). However, we empirically found that truncating the first $d(d+1)$ components generally achieves better performances.

The comparison results on *Oxford5k*, *Paris6k*, and *Holidays* datasets are reported in Table III. Firstly, we can observe that the democratic pooling [12] clearly outperforms sum/average-pooling on both FV [10] and VLAD [11] embedding methods. Secondly, our proposed masking schemes help to achieve considerable gains in performance across the variety of embedding and aggregating frameworks. Additionally, the MAX-mask generally provides higher performance boosts than the SUM/SIFT-mask, while SUM-mask and SIFT-mask give comparable results. At the comparison dimensionality $D = 4224$, the framework of $\phi_{\Delta} + \psi_d$ and $\phi_{\text{F-FAemb}} + \psi_d$ achieves comparable performances across various masking schemes and datasets. Hence we choose $\mathcal{M}_{*} + \phi_{\Delta} + \psi_d$ as our default framework for analyzing other parameters.

2) *Final feature dimensionality:* Different from recent works using convolutional features [8], [29], [34], [30], which have the final feature dimensionality upper bounded by the number of feature channels K of network architecture and selected layers, e.g., $K = 512$ for conv5 of VGG [18]. Taking the advantages of embedding methods, similar to NetVLAD [31], our proposed framework provides more flexibility on choosing the length of final representation.

Considering our default framework — $\mathcal{M}_{*} + \phi_{\Delta} + \psi_d$, we empirically set the number of retained PCA compo-

²We randomly select 5,000 images from the 100k Flickr image set [56].

TABLE IV: Number of retained PCA components (of local conv. features) and codebook size when varying the dimensionality. Note that for 512-D, PCA is applied to compress the aggregated representations.

Dim. D	512-D	1024-D	2048-D	4096-D	8064-D
PCA d	32	64	64	64	128
$ \mathcal{C} $	20	18	34	66	64

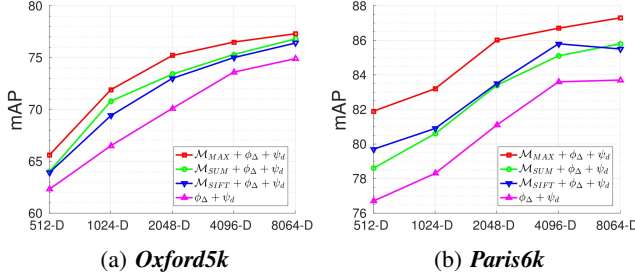


Fig. 5: Impact of the final representation dimensionality on *Oxford5k* and *Paris6k* datasets.

nents (of local conv. features) and the codebook size when varying the dimensionality in Table IV. For compact final representations of 512 dimensionality, we choose $d = 32$ to avoid using too few visual words which drastically degrades performance [12]. For longer final representations, i.e. 1024, 2048, 4096, imitating Fisher and VLAD presentations for SIFT features [74], we reduce local conv. features to $d = 64$. For the largest considered representation, i.e. 8064, imitating the Temb representation for SIFT features [12], we reduce local conv. features to $d = 128$. Note that the settings in Table IV are applied for all later experiments.

The Figure 5 shows the retrieval performance on two datasets, *Oxford5k* and *Paris6k*, when varying the final feature dimensionality. Unsurprisingly, the proposed method can boost the performance when increasing the final feature dimensionality. At 4096-D or higher, the improvements become small (or even decreased for $\mathcal{M}_{SIFT} + \phi_{\Delta} + \psi_d$ scheme on *Paris6k* dataset). In addition, we also observe that the masking schemes consistently help to gain extra performance across different dimensionalities.

3) *Image size*: Even though the authors in [30], [29] found that for the *Oxford5k* dataset, using the original size of images ($\max(W_I, H_I) = 1024$) provides best performance, it is necessary to evaluate the performance of our framework with a smaller image size since our framework highly depends on the number of local conv. features. Table V shows the retrieval performance on *Oxford5k* and *Paris6k* datasets with the image size of $\max(W_I, H_I) = 1024$ and $\max(W_I, H_I) = 724$. Similar to the reported results of [30] on *Oxford5k* dataset, we observe around 6-7% drop in mAP when scaling down images to $\max(W_I, H_I) = 724$ rather than the original images. While on *Paris6k* dataset, interestingly, the performances are more stable to the image size. We observe a small drop of 2.2% mAP on *Paris6k* dataset for R-MAC [30] with our experiments. These suggest that our method and R-MAC method [30] equivalently affected by the change in the image size.

The performance drops on *Oxford5k* can be explained that

TABLE V: Impact of input image size on *Oxford5k* and *Paris6k* datasets. The framework of $\mathcal{M}_{MAX/SUM} + \phi_{\Delta} + \psi_d$ is used to produce image representations.

Dim. D	$\max(W_I, H_I)$	Oxford5k		Paris6k	
		\mathcal{M}_{SUM}	\mathcal{M}_{MAX}	\mathcal{M}_{SUM}	\mathcal{M}_{MAX}
512	724	56.4	60.9	79.3	81.2
	1024	64.0	65.7	78.6	81.6

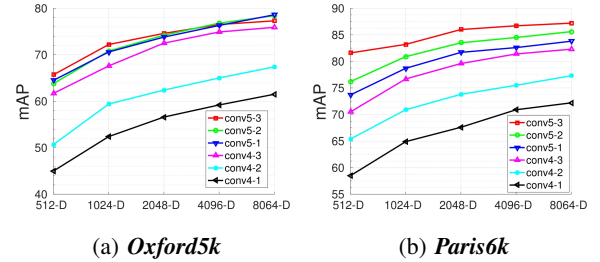


Fig. 6: Evaluation of retrieval performance of local deep conv. features from different layers on *Oxford5k* and *Paris6k* datasets. The framework of $\mathcal{M}_{MAX} + \phi_{\Delta} + \psi_d$ is used to produce image representations.

with bigger images, the CNN can take a closer “look” on smaller details in the images. Hence, the local conv. features can better distinguish details in different images. While the stable on *Paris6k* dataset can be perceived that the differences on these scenes are at global structures, i.e., a higher abstract level, rather than small details as on *Oxford5k* dataset. This explanation is also consistent with human understanding on these datasets.

4) *Layer selection*: In [8], the authors mentioned that deeper conv. layers produce features that are more reliable in differentiating images. Here, we re-evaluate this statement by comparing the retrieval performance (mAP) of features extracted from different conv. layers at the same dimensionality. In this experiment, we extract features from different conv. layers, including conv5-3, conv5-2, conv5-1, conv4-3, conv4-2, and conv4-1, following by a 2×2 max-pool layer with a stride of 2. The experimental results on *Oxford5k* and *Paris6k* datasets are shown in Figure 6. We observe that there are small drops in performance when using lower conv. layers until conv4-3. When going down further to conv4-2 and conv4-1, there are significant drops in performance. Regarding the pre-trained VGG network [18], this fact indicates that the last conv. layer (i.e., conv5-3) produces the most reliable representation for image retrieval.

Furthermore, as assembling multiple conv. layers of CNN would be beneficial [75] in localizing the saliency objects, we conduct additional experiments to evaluate whether combining different levels of abstraction from different conv. layers of CNN be useful for the retrieval task. Specifically, we concatenate feature maps from different layers as hyper-column feature maps which allow to normally use the proposed masking schemes. The experimental results are reported in VI, from which we observe that combining multiple conv. layers as hyper-column features helps to improve performances across many datasets, e.g., *Oxford5k*, *Paris6k*, and *Holidays*.

TABLE VI: Impact of combining multiple conv. layers as hyper-column feature maps on *Oxford5k*, *Paris6k*, and *Holidays* datasets. The framework of $\mathcal{M}_{\text{MAX}} + \phi_{\Delta(64,18)} + \psi_d$ is used to produce image representations, where $\phi_{\Delta(64,18)}$ denotes Temb with $d = 64$ and $|\mathcal{C}| = 18$.

conv5-3	conv5-2	conv5-1	Oxford5k	Paris6k	Holidays
✓			72.2	83.2	88.4
✓	✓		73.3	83.5	90.4
✓		✓	74.2	83.8	90.9
✓	✓	✓	74.8	84.5	90.8

5) *Binary representation framework*: In this section, we conduct experiments at a wide range of settings to find the setting that produces the best binary representation. As discussed in section V-B3 and V-B4, when using images of $\max(W_I, H_I) = 1024$, the last conv. layer of the VGG network [18], i.e., conv5-3, produces the most reliable representations. Hence, the default framework of $\mathcal{M}_{\text{MAX}} + \phi_{\Delta} + \psi_d$, in combination with these two settings (i.e., $\max(W_I, H_I) = 1024$ and conv5-3 features), is used to produce real-valued representations before passing forward to a hashing module. Furthermore, in the literature, unsupervised hashing methods are usually proposed to work with hand-crafted global image features, e.g., GIST [43], or deep learning features of a fully-connected layer, e.g., fc7 of AlexNet or VGG, it is unclear which method works the best with our proposed aggregated representations. Hence, we conduct experiments with various state-of-the-art unsupervised hashing methods including iterative quantization (ITQ) [35], relaxed binary autoencoder (RBA) [36], and K-means hashing (KMH) [70] to find the best hashing module for our framework.

The experimental results on *Oxford5k*, *Paris6k*, and *Holidays* datasets are presented in Table VII. There are some main observations from the results. Firstly, at the same code length, ITQ and RBA achieve comparable results, while both these methods significantly outperform KMH, on all datasets. Secondly, as discussed in Section V-B2, embedding local conv. features to higher dimensional space helps to enhance the discriminative power of the real-valued aggregated representation; however, as shown in Table VII, embedding to too high-dimensional space also causes information loss when producing compact binary codes, i.e., the best mAPs are achieved when the aggregated representation are at 512 or 1024 dimensions. The higher dimensional representations (i.e., 2048-D or 4096-D) cause the more mAPs loss. As embedding to 512-D, i.e., $\phi_{\Delta(32,20)}$, gives most stable results, we use this configuration in our final framework when producing binary representations.

C. Comparison to the state of the art

We thoroughly compare our proposed framework with state-of-the-art methods in the image retrieval task. We separate two experimental settings. The first experiment is when images are represented by mid-dimensional real-valued presentations. The second experiment is when images are represented by very compact representations, i.e., very short real-valued vectors or binary vectors.

1) *Comparison with the state of the art when images are represented by mid-dimensional real-valued vectors*: We report comparative results when images are represented by real-valued vectors in Table VIII. We separate two different settings, i.e., when deep features are extracted from an off-the-shelf pretrained network (i.e., VGG) or are extracted from a VGG network which is fine-tuned for the image retrieval task.

Using off-the-shelf VGG network [18]. The first observation is that at the dimensionality of 1024, our method using MAX-mask ($\mathcal{M}_{\text{MAX}} + \phi_{\Delta} + \psi_d$) achieves the highest mAP in comparison to recent deep learning-based methods [8], [29], [34], [30], [31] acrossing different datasets. The second observation is that by combining multiple conv. layers, conv5-3, conv5-2, and conv5-1, denoted as $\mathcal{M}_{\text{MAX}(\text{conv5-3,2,1})}$, the proposed MAX scheme consistently boosts the retrieval accuracy. Our framework ($\mathcal{M}_{\text{MAX}(\text{conv5-3,2,1})} + \phi_{\Delta} + \psi_d$) with dimensionality of 512 is competitive with other state-of-the-art methods [29], [30]. In particular, in comparison with CroW [29], while having slightly lower performances in *Oxford5k*, our method outperforms CroW on *Paris6k* and *Holidays*. In comparison with R-MAC [30], the proposed framework outperforms RMAC on *Oxford5k* and *Holidays* datasets, while it is comparable to RMAC on *Paris6k* dataset. Note that some compared methods, e.g., siaMAC [34], R-MAC [30], SPoC [8], CroW [29] have the dimensionality of 512 or 256. This is because the final feature dimensionality of these methods is upper bounded by the number of feature channels K of network architecture and selected layers, e.g., $K = 512$ for conv5 of VGG16. While our proposed method provides more flexibility in the feature length, thanks to the embedding process.

We note that it is unclear in the performance gain when increasing the length of the final representation in R-MAC [30] or CRoW [29] (e.g., by increasing the number of feature maps in conv. layers, even at the cost of a significant increase in the number of CNN parameters and the additional efforts of re-training. In fact, in [44], the authors design an experiment to investigate whether increasing the number feature maps of the conv. layer before the fully connected one in which the representation is extracted, would help to increase the performance of various visual tasks, including image classification, attribute detection, fine-grained recognition, and instance retrieval. Interestingly, the experimental results show that while the performance increases on other tasks, it degrades on the retrieval one. The authors explain that the more powerful the network is, the more generality it can provide. As a result, the representation becomes more invariant to instance level differences. Even though, in that experiment, the image representation is constructed from a fully-connected layer, which is different from our current context using conv. layer, the explanation in [44] could still be applicable. This raises the question about the retrieval performance when increasing the number of feature maps of conv. layers as a way to increase final representation dimensionality in compared deep-based retrieval methods SPoC [8], R-MAC [30], or CRoW [29]. It is worth noting that NetVLAD [31] and MOP-CNN [40]

TABLE VII: Comparison of different frameworks when the final representations are binary values. The values in brackets in **Embedding** column indicate the dimension of local conv. features after PCA and the codebook size, respectively. **Dim.** column indicates the dimension of real-valued representations before subjecting into a hash function. We evaluate the binary representations at code lengths 64, 128, 256, 512 with three state-of-the-art unsupervised hashing methods ITQ [35], RBA [36], and KMH [70]. Results are reported on *Oxford5k*, *Paris6k* and *Holidays* dataset.

Hashing	Embedding	Dim.	Oxford5k				Paris6k				Holidays			
			64	128	256	512	64	128	256	512	64	128	256	512
ITQ [35]	$\phi_{\Delta}(32,20)$	512	18.3	31.6	45.0	57.3	32.9	49.7	63.0	74.7	57.5	70.7	79.5	83.5
	$\phi_{\Delta}(64,18)$	1024	18.7	29.5	42.9	55.8	33.5	49.0	61.0	72.4	58.7	71.5	79.4	82.9
	$\phi_{\Delta}(64,34)$	2048	18.3	27.7	38.4	50.3	28.4	44.3	57.9	68.6	57.9	71.1	79.1	82.3
	$\phi_{\Delta}(64,66)$	4096	16.0	23.0	33.6	45.8	26.1	40.1	52.9	65.4	56.1	70.2	78.8	80.5
RBA [36]	$\phi_{\Delta}(32,20)$	512	17.8	31.3	45.3	57.1	31.5	50.8	63.7	74.9	56.7	71.6	78.5	83.2
	$\phi_{\Delta}(64,18)$	1024	18.4	30.1	42.7	55.7	32.8	49.4	61.3	72.8	57.6	71.1	79.3	82.7
	$\phi_{\Delta}(64,34)$	2048	17.3	30.9	39.1	53.5	29.0	45.0	59.1	68.6	57.1	70.8	78.8	81.8
	$\phi_{\Delta}(64,66)$	4096	15.7	25.1	39.0	48.3	25.8	39.3	55.6	64.6	55.6	67.5	77.5	80.1
KMH [70]	$\phi_{\Delta}(32,20)$	512	18.5	26.5	39.1	54.4	32.0	45.7	61.6	75.3	53.4	65.0	75.0	80.8
	$\phi_{\Delta}(64,18)$	1024	18.1	28.1	41.4	53.5	30.0	48.3	61.4	73.7	54.6	68.0	78.0	82.4
	$\phi_{\Delta}(64,34)$	2048	15.7	26.7	38.5	51.4	26.0	40.8	56.7	69.2	51.2	68.4	76.4	81.2
	$\phi_{\Delta}(64,66)$	4096	13.4	20.7	31.2	47.0	21.1	33.3	49.8	63.7	50.0	63.2	72.8	80.1

TABLE VIII: Comparison with the state of the art when the final representations are real values. The results of compared methods are cited from the corresponding papers when available. For results of R-MAC[30] on Holidays and Holidays+Flickr1M, we use the released code of R-MAC[30] to evaluate on these datasets.

	Method	Dim.	Size (Byte)	Datasets					
				<i>Oxford5k</i>	<i>Oxford105k</i>	<i>Paris6k</i>	<i>Paris106k</i>	<i>Holidays</i>	<i>Hol.+F1M</i>
SIFT	$\phi_{\Delta} + \psi_d$ [12]	512	2k	52.8	46.1	-	-	61.7	46.9
	$\phi_{\Delta} + \psi_d$ [12]	1024	4k	56.0	50.2	-	-	72.0	49.4
	ϕ_F -FAemb + ψ_d [14]	512	2k	53.9	50.9	-	-	69.0	65.3
	ϕ_F -FAemb + ψ_d [14]	1024	4k	58.2	53.2	-	-	70.8	68.5
Off-the-shelf network	SPoC [8]	256	1k	53.1	-	50.1	-	80.2	-
	MOP-CNN [40]	512	2k	-	-	-	-	78.4	-
	CroW [29]	512	2k	70.8	65.3	79.7	72.2	85.1	-
	MAC [34]	512	2k	56.4	47.8	72.3	58.0	76.7	-
	R-MAC [30]	512	2k	66.9	61.6	83.0	75.7	86.6	71.5
	NetVLAD [31]	1024	4k	62.6	-	73.3	-	87.3	-
	NetVLAD [31]	4096	16k	66.6	-	77.4	-	88.3	-
	$\mathcal{M}_{\text{SIFT}} + \phi_{\Delta} + \psi_d$	512	2k	64.4	59.4	79.5	70.6	86.5	-
	$\mathcal{M}_{\text{SUM}} + \phi_{\Delta} + \psi_d$	512	2k	64.0	58.8	78.6	70.4	86.4	-
	$\mathcal{M}_{\text{MAX}} + \phi_{\Delta} + \psi_d$	512	2k	65.7	60.5	81.6	72.4	85.0	71.9
	$\mathcal{M}_{\text{MAX}(\text{conv5-3,2,1})} + \phi_{\Delta} + \psi_d$	512	2k	69.2	65.3	82.5	74.0	88.7	73.0
	$\mathcal{M}_{\text{SIFT}} + \phi_{\Delta} + \psi_d$	1024	4k	69.9	64.3	81.7	73.8	87.1	-
	$\mathcal{M}_{\text{SUM}} + \phi_{\Delta} + \psi_d$	1024	4k	70.8	64.4	80.6	73.8	86.9	-
	$\mathcal{M}_{\text{MAX}} + \phi_{\Delta} + \psi_d$	1024	4k	72.2	67.9	83.2	76.1	88.4	79.1
	$\mathcal{M}_{\text{MAX}(\text{conv5-3,2,1})} + \phi_{\Delta} + \psi_d$	1024	4k	74.8	70.4	84.5	78.6	90.8	81.7
Finetuned network	siaMAC + MAC [34]	512	2k	79.7	73.9	82.4	74.6	79.5	-
	siaMAC + R-MAC [34]	512	2k	77.0	69.2	83.8	76.4	82.5	-
	NetVLAD* [31]	1024	4k	69.2	-	76.5	-	86.5	-
	NetVLAD* [31]	4096	16k	71.6	-	79.7	-	87.5	-
	siaMAC[34] + $\mathcal{M}_{\text{MAX}} + \phi_{\Delta} + \psi_d$	512	2k	77.7	72.7	83.2	76.5	86.3	-
	siaMAC[34] + $\mathcal{M}_{\text{MAX}} + \phi_{\Delta} + \psi_d$	1024	4k	81.4	77.4	84.8	78.9	88.9	82.1
	NetVLAD* [31] + $\mathcal{M}_{\text{MAX}} + \phi_{\Delta} + \psi_d$	1024	4k	75.2	71.7	84.4	76.9	91.5	-
	NetVLAD* [31] + $\mathcal{M}_{\text{MAX}} + \phi_{\Delta} + \psi_d$	4096	16k	78.2	75.7	87.8	81.8	92.2	-
	siaMAC[34] + $\mathcal{M}_{\text{MAX}} + \phi_{\Delta} + \psi_d$	4096	16k	83.8	80.6	88.3	83.1	90.1	-

TABLE IX: Comparison with the state of the art on very compact representations. (re.) and (bin.) mean that the representations are real values and binary values, respectively. The distance measures are shown in **Dist.** column.

Method	Dim.	Size (Byte)	Dist.	Datasets				
				<i>Oxford5k</i>	<i>Oxford105k</i>	<i>Paris6k</i>	<i>Paris106k</i>	<i>Holidays</i>
siaMAC + MAC [34]	16 (re.)	64	Cosine	56.2	45.5	57.3	43.4	51.3
siaMAC + R-MAC [34]	16 (re.)	64	Cosine	46.9	37.9	58.8	45.6	54.4
GeM [49]	16 (re.)	64	Cosine	56.2	44.4	63.5	45.5	60.9
$\mathcal{M}_{\text{MAX}} + \phi_{\Delta}(32,20) + \psi_d + \text{ITQ}$	256 (bin.)	32	Hamming	45.0	38.3	63.0	50.5	79.5
$\mathcal{M}_{\text{MAX}} + \phi_{\Delta}(32,20) + \psi_d + \text{ITQ}$	512 (bin.)	64	Hamming	57.3	49.8	74.7	56.1	83.5
siaMAC \dagger + $\mathcal{M}_{\text{MAX}} + \phi_{\Delta}(32,20) + \psi_d + \text{ITQ}$	256 (bin.)	32	Hamming	58.5	49.1	74.1	63.6	79.9
siaMAC \dagger + $\mathcal{M}_{\text{MAX}} + \phi_{\Delta}(32,20) + \psi_d + \text{ITQ}$	512 (bin.)	64	Hamming	68.9	60.9	79.1	70.3	83.6

methods can also produce higher dimensional representation by increasing the codebook size. However, as shown in Table VIII at comparable dimensions, the proposed framework clearly outperforms these methods.

Taking advantages of fine-tuned VGG networks. Since our proposed framework takes the 3D activation tensor of a conv. layer as the input, it is totally compatible with deep networks which are fine-tuned for image retrieval task such as siaMAC [34] and NetVLAD [31] (noted as NetVLAD \star). In the “Fine-tuned network” section of Table VIII, we evaluate our best framework — $\mathcal{M}_{MAX} + \phi_{\Delta} + \psi_d$ in which the local conv. features of the fine-tuned VGG networks NetVLAD \star [31], siaMAC [34] are used as inputs.

The experimental results from Table VIII show that, for our $\mathcal{M}_{MAX} + \phi_{\Delta} + \psi_d$ framework, using conv. features from the siaMAC network usually give better performance than using those from the NetVLAD \star network. When using local conv. features extracted from the fine-tuned network siaMAC [34], our method is competitive to **siaMAC + R-MAC** and **siaMAC + MAC** [34] at dimensionality of 512. At 1024 dimensions, our method consistently outperforms both siaMAC and NetVLAD \star on all datasets. These considerable improvements indicate that our proposed framework can fully utilize the discrimination gain of local conv. features achieved by those fine-tuning networks.

Very large scale image retrieval. In order to verify the capabilities of our framework in real scenarios, we now evaluate it with a very large scale dataset, *Holidays+Flickr1M*. The experimental results show that the proposed framework “siaMAC + $\mathcal{M}_{MAX} + \phi_{\Delta} + \psi_d$ ” is quite robust to the database size, i.e., when adding 1M distractor images to the Holidays dataset, the performance drop is only about 7%. We achieve a mAP of 82.1 which is significantly higher than 71.5 of the R-MAC [30].

2) *Comparison with the state of the art when images are represented by very compact representations:* We now compare the quality of binary image representations producing by our framework with compact real-valued representations from state-of-the-art methods at comparable sizes (in Bytes) [34], [49]. Furthermore, ITQ [35] is used as the hashing function in our final framework as it gives competitive results (Section V-B5) and it is also computationally efficient in both training and producing new binary codes. The comparative results are reported in Table IX.

First of all, it is clear that at the same image descriptor size, e.g., 64 bytes, even when using off-the-shelf VGG [18], our framework significantly outperforms [34], [49] which use fine-tuned VGG networks. For examples, the proposed framework outperforms the second best GeM [49] large margins, i.e., +11.2% and +22.6% on *Paris6k* and *Holidays* datasets, respectively. Secondly, when using local conv. features of a fine-tuned VGG, e.g., siaMAC [34], our framework achieves significant extra improvements in retrieval performances over all datasets.

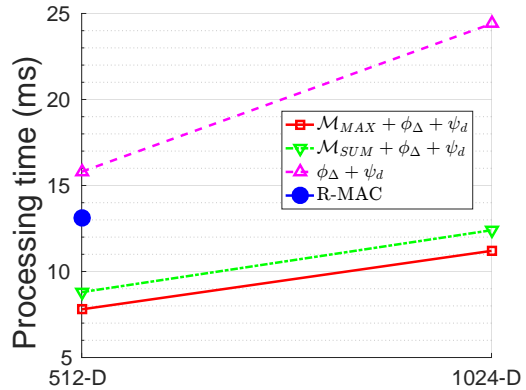


Fig. 7: The averaged online processing time of 5063 images of *Oxford5k* dataset.

D. Processing time

We empirically evaluate the online processing time of our proposed framework. We also compare the online processing time between our proposed framework and one of the most competitive methods: R-MAC [30]. Both implementations of our framework and R-MAC are in Matlab. The experiments are carried out on a processor core (i7-6700 CPU @ 3.40GHz). The reported processing time in Fig. 7 is the averaged on-line processing times of 5063 images of *Oxford5k* dataset, excluding the time for feature extraction. This figure shows that by applying MAX/SUM-mask, our proposed framework can significantly reduce the computational cost. It is because the proposed masking schemes help to remove about 70% (for MAX-mask) and 50% (for SUM-mask) of local conv. features (Section III-C). Additionally, at the dimensionality 512, our framework $\mathcal{M}_{MAX/SUM} + \phi_{\Delta} + \psi_d$ is computationally faster than R-MAC [30].

VI. CONCLUSION

In this paper, we present an effective framework which takes activations of a convolutional layer as the input and produces highly-discriminative image representation for image retrieval. In the proposed framework, we propose to enhance discriminative power of the image representation in two main steps: (i) selecting a representative set of local conv. features using our proposed masking schemes, including SIFT/SUM/MAX-mask, then (ii) embedding and aggregating using the state-of-art methods [12], [13]. In order to make the final representations suitable for large scale search, we further compress the real-valued representation by cascading a hashing function into framework. We comprehensively evaluate and analysis each component in the framework to figure out the best configuration. Solid experimental results show that the proposed framework compares favorably with the state-of-the-art for real-valued representations. Moreover, our binary representations are significantly outperforms the state-of-the-art methods at comparable sizes.

REFERENCES

- [1] G. Quellec, M. Lamard, G. Cazuguel, B. Cochener, and C. Roux, "Adaptive nonseparable wavelet transform via lifting and its application to content-based image retrieval," *TIP*, vol. 19, no. 1, pp. 25–35, Jan 2010.
- [2] W. Bian and D. Tao, "Biased discriminant euclidean embedding for content-based image retrieval," *TIP*, vol. 19, no. 2, pp. 545–554, Feb 2010.
- [3] X. Li, Y. Ye, and M. K. Ng, "MultiVCRank with applications to image retrieval," *TIP*, vol. 25, no. 3, pp. 1396–1409, March 2016.
- [4] R. Hong, L. Li, J. Cai, D. Tao, M. Wang, and Q. Tian, "Coherent semantic-visual indexing for large-scale image retrieval in the cloud," *TIP*, vol. 26, no. 9, pp. 4128–4138, Sept 2017.
- [5] Y. Wang, X. Lin, L. Wu, and W. Zhang, "Effective multi-query expansions: Collaborative deep networks for robust landmark retrieval," *TIP*, vol. 26, no. 3, pp. 1393–1404, March 2017.
- [6] D. G. Lowe, "Object recognition from local scale-invariant features," in *ICCV*, 1999.
- [7] R. Arandjelović and A. Zisserman, "Three things everyone should know to improve object retrieval," in *CVPR*, 2012.
- [8] A. Babenko and V. Lempitsky, "Aggregating local deep features for image retrieval," in *ICCV*, 2015.
- [9] J. Sivic, A. Zisserman *et al.*, "Video google: a text retrieval approach to object matching in videos," in *ICCV*, 2003.
- [10] F. Perronnin and C. Dance, "Fisher kernels on visual vocabularies for image categorization," in *CVPR*, 2007.
- [11] H. Jégou, M. Douze, C. Schmid, and P. Pérez, "Aggregating local descriptors into a compact image representation," in *CVPR*, 2010.
- [12] H. Jégou and A. Zisserman, "Triangulation embedding and democratic aggregation for image search," in *CVPR*, 2014.
- [13] T.-T. Do, Q. Tran, and N.-M. Cheung, "FAemb: A function approximation-based embedding method for image retrieval," in *CVPR*, 2015.
- [14] T.-T. Do and N.-M. Cheung, "Embedding based on function approximation for large scale image search," *TPAMI*, 2017.
- [15] H. Jégou, M. Douze, and C. Schmid, "On the burstiness of visual elements," in *CVPR*, 2009.
- [16] J. Delhumeau, P.-H. Gosselin, H. Jégou, and P. Pérez, "Revisiting the vlad image representation," in *ACM MM*, 2013.
- [17] A. Krizhevsky, I. Sutskever, and G. E. Hinton, "Imagenet classification with deep convolutional neural networks," in *NIPS*, 2012.
- [18] K. Simonyan and A. Zisserman, "Very deep convolutional networks for large-scale image recognition," *arXiv preprint arXiv:1409.1556*, 2014.
- [19] C. Szegedy, W. Liu, Y. Jia, P. Sermanet, S. Reed, D. Anguelov, D. Erhan, V. Vanhoucke, and A. Rabinovich, "Going deeper with convolutions," in *CVPR*, 2015.
- [20] K. He, X. Zhang, S. Ren, and J. Sun, "Deep residual learning for image recognition," *arXiv preprint arXiv:1512.03385*, 2015.
- [21] R. Girshick, J. Donahue, T. Darrell, and J. Malik, "Rich feature hierarchies for accurate object detection and semantic segmentation," in *CVPR*, 2014.
- [22] S. Ren, K. He, R. Girshick, and J. Sun, "Faster R-CNN: Towards real-time object detection with region proposal networks," in *NIPS*, 2015.
- [23] Y. Cao, C. Shen, and H. T. Shen, "Exploiting depth from single monocular images for object detection and semantic segmentation," *TIP*, vol. 26, no. 2, pp. 836–846, Feb 2017.
- [24] Y. Li, S. Tang, M. Lin, Y. Zhang, J. Li, and S. Yan, "Implicit negative sub-categorization and sink diversion for object detection," *TIP*, vol. 27, no. 4, pp. 1561–1574, April 2018.
- [25] G. Lin, C. Shen, I. D. Reid, and A. van den Hengel, "Efficient piecewise training of deep structured models for semantic segmentation," in *CVPR*, 2015.
- [26] T.-T. Do, A. Nguyen, I. D. Reid, D. G. Caldwell, and N. G. Tsagarakis, "Affordancenet: An end-to-end deep learning approach for object affordance detection," in *ICRA*, 2018.
- [27] K. He, G. Gkioxari, P. Dollár, and R. B. Girshick, "Mask R-CNN," in *ICCV*, 2017.
- [28] O. Russakovsky, J. Deng, H. Su, J. Krause, S. Satheesh, S. Ma, Z. Huang, A. Karpathy, A. Khosla, M. Bernstein, A. C. Berg, and L. Fei-Fei, "ImageNet Large Scale Visual Recognition Challenge," *IJCV*, vol. 115, no. 3, pp. 211–252, 2015.
- [29] Y. Kalantidis, C. Mellina, and S. Osindero, "Cross-dimensional weighting for aggregated deep convolutional features," in *ECCV Workshops*, 2016.
- [30] G. Tolias, R. Sire, and H. Jégou, "Particular object retrieval with integral max-pooling of CNN activations," in *ICLR*, 2016.
- [31] R. Arandjelović, P. Gronat, A. Torii, T. Pajdla, and J. Sivic, "NetVLAD: CNN architecture for weakly supervised place recognition," in *CVPR*, 2016.
- [32] Y. Li, X. Kong, L. Zheng, and Q. Tian, "Exploiting hierarchical activations of neural network for image retrieval," in *ACM MM*, 2016.
- [33] X. S. Wei, J. H. Luo, J. Wu, and Z. H. Zhou, "Selective convolutional descriptor aggregation for fine-grained image retrieval," *TIP*, vol. 26, pp. 2868–2881, June 2017.
- [34] F. Radenović, G. Tolias, and O. Chum, "CNN image retrieval learns from BoW: Unsupervised fine-tuning with hard examples," in *ECCV*, 2016.
- [35] Y. Gong, S. Lazebnik, A. Gordo, and F. Perronnin, "Iterative quantization: A procrustean approach to learning binary codes for large-scale image retrieval," *TPAMI*, pp. 2916–2929, 2013.
- [36] T.-T. Do, D.-K. Le Tan, T. T. Pham, and N.-M. Cheung, "Simultaneous feature aggregating and hashing for large-scale image search," in *CVPR*, 2017.
- [37] T. Hoang, T.-T. Do, D.-K. L. Tan, and N.-M. Cheung, "Selective deep convolutional features for image retrieval," in *ACM-MM*, 2017.
- [38] H. Jégou, M. Douze, and C. Schmid, "Hamming embedding and weak geometric consistency for large scale image search," in *ECCV*, 2008.
- [39] A. S. Razavian, H. Azizpour, J. Sullivan, and Y. Carlsson, "CNN features off-the-shelf: An astounding baseline for recognition," in *CVPRW*, 2014.
- [40] Y. Gong, L. Wang, R. Guo, and S. Lazebnik, "Multi-scale orderless pooling of deep convolutional activation features," in *ECCV*, 2014.
- [41] K. Yan, Y. Wang, D. Liang, T. Huang, and Y. Tian, "SIFT for image retrieval: Alternative or complementary?" in *ACM MM*, 2016.
- [42] Z. Liu, S. Wang, L. Zheng, and Q. Tian, "Robust imagegraph: Rank-level feature fusion for image search," *TIP*, vol. 26, no. 7, pp. 3128–3141, July 2017.
- [43] A. Oliva and A. Torralba, "Modeling the shape of the scene: A holistic representation of the spatial envelope," *IJCV*, pp. 145–175, 2001.
- [44] H. Azizpour, A. S. Razavian, J. Sullivan, A. Maki, and S. Carlsson, "From generic to specific deep representations for visual recognition," in *CVPR Workshops*, 2015.
- [45] A. Babenko, A. Slesarev, A. Chigorin, and V. Lempitsky, "Neural codes for image retrieval," in *ECCV*, 2014.
- [46] J. Cao, Z. Huang, P. Wang, C. Li, X. Sun, and H. T. Shen, "Quartet-net learning for visual instance retrieval," in *ACM MM*, 2016.
- [47] B. Thomee, D. A. Shamma, G. Friedland, B. Elizalde, K. Ni, D. Poland, D. Borth, and L.-J. Li, "YFCC100M: The new data in multimedia research," *Communications of the ACM*, vol. 59, no. 2, pp. 64–73, 2016.
- [48] Y. Zhang, J. Wu, and J. Cai, "Compact representation of high-dimensional feature vectors for large-scale image recognition and retrieval," *TIP*, vol. 25, no. 5, May 2016.
- [49] F. Radenović, G. Tolias, and O. Chum, "Fine-tuning CNN image retrieval with no human annotation," in *arXiv:1711.02512*, 2017.
- [50] A. Gordo, J. Almazán, J. Revaud, and D. Larlus, "End-to-End learning of deep visual representations for image retrieval," *IJCV*, 2017.
- [51] H. Jégou, M. Douze, and C. Schmid, "Product quantization for nearest neighbor search," *TPAMI*, pp. 117–128, 2011.
- [52] M. Douze, H. Jégou, and F. Perronnin, "Polysemous codes," in *ECCV*, 2016.
- [53] H. Jégou and O. Chum, "Negative evidences and co-occurrences in image retrieval: The benefit of PCA and Whitening," in *ECCV*, 2012.
- [54] G. Tolias, Y. Avrithis, and H. Jégou, "To aggregate or not to aggregate: Selective match kernels for image search," in *ICCV*, 2013.
- [55] M. D. Zeiler and R. Fergus, "Visualizing and understanding convolutional networks," *CoRR*, vol. abs/1311.2901, 2013. [Online]. Available: <http://arxiv.org/abs/1311.2901>
- [56] J. Philbin, O. Chum, M. Isard, J. Sivic, and A. Zisserman, "Object retrieval with large vocabularies and fast spatial matching," in *CVPR*, 2007.
- [57] —, "Lost in quantization: Improving particular object retrieval in large scale image databases," in *CVPR*, 2008.
- [58] H. Jégou, M. Douze, and C. Schmid, "Improving bag-of-features for large scale image search," *IJCV*, vol. 87, no. 3, pp. 316–336, May 2010.
- [59] K. Yu and T. Zhang, "Improved Local Coordinate Coding using Local Tangents," in *ICML*, 2010.
- [60] R. Negrel, D. Picard, and P. Gosselin, "Web scale image retrieval using compact tensor aggregation of visual descriptors," in *MultiMedia*, vol. 20, no. 3. IEEE, 2013, pp. 24–33.
- [61] Y.-L. Boureau, J. Ponce, and Y. Lecun, "A theoretical analysis of feature pooling in visual recognition," in *ICML*, 2010.
- [62] N. Murray and F. Perronnin, "Generalized max pooling," in *CVPR*, 2014.
- [63] F. Perronnin, J. Sánchez, and T. Mensink, "Improving the fisher kernel for large-scale image classification," in *ECCV*, 2010.

- [64] K. Grauman and R. Fergus, “Learning binary hash codes for large-scale image search,” *Machine Learning for Computer Vision*, 2013.
- [65] J. Wang, T. Zhang, J. Song, N. Sebe, and H. T. Shen, “A survey on learning to hash,” *TPAMI*, 2017.
- [66] M. A. Carreira-Perpinan and R. Razi-perchikolaei, “Hashing with binary autoencoders,” in *CVPR*, 2015.
- [67] T.-T. Do, A.-D. Doan, and N.-M. Cheung, “Learning to hash with binary deep neural network,” in *ECCV*, 2016.
- [68] Y. Weiss, A. Torralba, and R. Fergus, “Spectral hashing,” in *NIPS*, 2008.
- [69] T.-T. Do, A.-D. Doan, D.-T. Nguyen, and N.-M. Cheung, “Binary hashing with semidefinite relaxation and augmented lagrangian,” in *ECCV*, 2016.
- [70] K. He, F. Wen, and J. Sun, “K-means hashing: An affinity-preserving quantization method for learning binary compact codes,” in *CVPR*, 2013.
- [71] A. Gordo, J. Almazan, J. Revaud, and D. Larlus, “Deep image retrieval: Learning global representations for image search,” in *ECCV*, 2016.
- [72] A. Vedaldi and K. Lenc, “Matconvnet - convolutional neural networks for MATLAB,” *CoRR*, vol. abs/1412.4564, 2014. [Online]. Available: <http://arxiv.org/abs/1412.4564>
- [73] A. Vedaldi and B. Fulkerson, “VLFeat: An open and portable library of computer vision algorithms,” in *ACM-MM*, 2010.
- [74] H. Jégou, F. Perronnin, M. Douze, J. Sánchez, P. Pérez, and C. Schmid, “Aggregating local image descriptors into compact codes,” *TPAMI*, pp. 1704–1716, 2012.
- [75] B. Hariharan, P. Arbelaz, R. Girshick, and J. Malik, “Hypercolumns for object segmentation and fine-grained localization,” in *CVPR*, 2014.